Microscopic Model Analyses of the Elastic Scattering of 25, 30 and 40 MeV Protons from Targets of Diverse Mass

P. K. Deb,[A] *K. Amos*[A] *and S. Karataglidis*[B]

[A] School of Physics, University of Melbourne,
Victoria 3010, Australia.
[B] Theory Division, Los Alamos National Laboratory,
Los Alamos, New Mexico, 87545, USA.

Abstract

An extensive survey and analysis of cross-section and analysing power data from proton elastic scattering at energies 25 to 40 MeV is presented. The data are compared with predictions obtained from a full folding specification of the proton–nucleus optical potentials. Isotope and energy variation of the data is explained.

1. Introduction

The development of a fully microscopic, coordinate space optical model to analyse proton scattering from nuclei enables predictions to be made of proton elastic and, via a distorted wave approximation (DWA), of inelastic scattering. All details of the procedure have been given in a recent review (Amos *et al.* 2000). In particular, with this approach, successful analyses have been made of proton–nucleus (pA) elastic scattering data taken at 65 and 200 MeV (Dortmans *et al.* 1997, 1998) and from targets of diverse mass and elastic and inelastic p-^{12}C scattering data at 200 MeV have been understood (Dortmans *et al.* 1995). Very recently two-nucleon (NN) effective interactions have been specified with which on folding with wave functions from a complete $(0 + 2)\hbar\omega$ shell model calculation, gave (g-folding) optical potentials for proton energies from 40 to 800 MeV. With those potentials, elastic p-^{12}C scattering with energies in that extensive range were reproduced quite well (Deb and Amos 2000).

Herein we present the results of analyses of the elastic scattering of 25, 30 and 40 MeV protons from many nuclei (^{6}Li to ^{238}U) and made using coordinate space optical potentials formed by g-folding, i.e. by folding complex energy-dependent effective NN interactions with ground state density matrices given by shell model descriptions of those nuclei. A select few of the results presented in this study have been used in a brief report (Deb *et al.* 2000), the purpose of which was to establish the propriety of the NN effective interactions in this energy regime. The interest to find a credible prescription of the optical potentials at these energies lies with current and future analyses of data from the scattering of $25A$, $30A$ and $40A$ MeV radioactive ions from hydrogen targets. Such experiments are being made at many facilities throughout the world (Auger *et al.* 1999; Mueller 1999; Tanihata 1999). Also g-folding optical potentials are required to define the distorted waves in 'no parameter' DWA analyses of the cross sections from the inelastic excitation of the radioactive ions. Measurements and subsequent analyses of such inelastic excitations are feasible and have been made recently (Lagoyannis *et al.* 2001) for the excitation of the 2^+ (1.8 MeV) state in ^{6}He.

At the energies considered in the present work (25, 30 and 40 MeV), collective structures in the response function of a nucleus may contribute above any specific microscopic description based on an effective *NN* multiple scattering theory. For example, if the energy is consistent with excitation of a giant resonance, virtual excitation of that resonance could contribute to the scattering. Indeed past studies (von Geramb *et al.* 1975) indicated that such virtual excitation of the giant resonances gives energy-dependent signatures in cross sections. Those effects however are of the order of $1 \, \text{mb} \, \text{sr}^{-1}$ at most and so are evident, basically, only at large momentum transfers for elastic scattering. The usual (phenomenological) optical potential sufficed to give the bulk of the (elastic) scattering results in that past study (von Geramb *et al.* 1975). Hence, notwithstanding interference effects, a first-order microscopic description of the optical potential, based on single-site *NN* scattering in medium, could still produce good agreement with elastic scattering data of magnitude greater than a few tenths of a $\text{mb} \, \text{sr}^{-1}$ taken for energies in the range 25 to 40 MeV.

Still, at these energies the specific character of the target response may be needed to specify appropriately the effective *NN* interaction one should use in the *g*-folding process. If so, the standard prescription we have used to date to define the effective interactions may need some modification. Calculations at these energies using that standard prescription and comparison with data would calibrate any such required modifications. Of course, if the specific response function effects in the definition of the effective *NN* interaction are of sufficient import, their omission should be evident in the comparisons of current model results with data from light mass targets first, and at 25 MeV in particular, given the excitation energies of the giant resonances and the variation of those excitation energies with target mass. Therefore, we have analysed proton elastic scattering data taken in the range of energies 25 to 40 MeV and from a number of nuclei in the mass range $A = 6$ to 238. The method used was that with which successful analyses of cross-section and spin-dependent data from 65 and 200 MeV proton scattering have been made from many nuclei ranging in mass from ^{3}He to ^{238}U (Dortmans *et al.* 1997, 1998). As with those studies, all details of the effective interactions and structure required to define the (complex, non-local) optical potentials are preset and no *a posteriori* adjustment or simplifying approximation is made to the complex non-local optical potentials that result from the *g*-folding process.

We consider herein only the elastic scattering channel. At and about 25 MeV proton energy we have considered 18 targets for elastic scattering cross sections, namely ^{6,7}Li, ^{12}C, ^{14}N, ^{18}O, ^{24}Mg, ^{27}Al, ^{28}Si, ^{40,42,44,48}Ca, ^{58}Cu, ^{88}Sr, ^{89}Y, ^{152}Sm, ^{232}Th and ^{238}U. At that energy we have analysed the data from eight targets for which analysing powers have been taken, namely ^{12}C, ^{18}O, ^{24}Mg, ^{28}Si, ^{32}S, ^{88}Sr, ^{118}Sn and ^{152}Sm. At and about 30 MeV proton energy, we have considered 20 targets for elastic differential cross sections, namely ^{10}B, ^{13}C, ^{16}O, ^{20}Ne, ^{40}Ar, ^{56}Fe, ^{58}Ni, ^{63}Cu, ^{66}Zn, ^{90}Zr, ^{112,116,120,122,124}Sn, ^{139}La, ^{144}Sm, ^{176}Yb, ^{208}Pb and ^{209}Bi, and 14 targets for analysing powers, namely ^{9}Be, ^{10}B, ^{13}C, ^{16}O, ^{40}Ar, ^{54,56}Fe, ^{58}Ni, ^{65}Cu, ^{90}Zr, ^{92}Mo, ^{120}Sn, ^{176}Yb and ^{208}Pb. At 40 MeV, we have considered 19 targets for differential cross sections, namely ^{6}Li, ^{12}C, ^{16}O, ^{24}Mg, ^{27}Al, ^{28}Si, ^{40}Ca, ^{58,60,62,64}Ni, ^{64}Zn, ^{90}Zr, ^{116,118,120,122,124}Sn and ^{208}Pb, and 14 targets for analysing powers, namely ^{12}C, ^{40}Ca, ^{58,60,62,64}Ni, ^{64}Zn, ^{90}Zr, ^{116,118,120,122,124}Sn and ^{208}Pb. We compare predictions from the optical potentials defined for each target with the proton elastic scattering experimental data that are available.

The paper is arranged as follows: A brief discussion of the procedure for obtaining our microscopic optical potentials is given in Section 2. In Section 3 we present and discuss the results for the scattering of protons from those nuclei considered in the present study while conclusions that may be drawn are presented in Section 4.

2. The Microscopic Optical Potential

As a detailed presentation of the coordinate space microscopic optical potential has been published (Amos *et al.* 2000), only salient features are given herein.

(2a) The g-Folding Process

Nucleon–nucleus (*NA*) elastic scattering is specified in terms of the scattering phase shifts which may be extracted from the asymptotic behaviour of solutions of Schrödinger equations,

$$\left[\frac{\hbar^2}{2\mu} \nabla^2 - V_c(r) + E \right] \Psi(\mathbf{r}) = \int U(\mathbf{r}, \mathbf{r}'; E) \Psi(\mathbf{r}') \, d\mathbf{r}', \tag{1}$$

where, with $\mathbf{r}, \mathbf{r}'$ being relative *NA* coordinates, $V_c(r)$ is a Coulomb interaction (usually taken to be that associated with a uniform charge distribution), and $U(\mathbf{r}, \mathbf{r}')$ is the optical potential which in general should be non-local, complex and energy dependent. Partial wave expansions give the Schrödinger equations as

$$\left[\frac{\hbar^2}{2\mu} \left\{ \frac{d^2}{dr^2} - \frac{l(l+1)}{r^2} \right\} - V_c(r) + E \right] \chi_l(k, r) = \int_0^\infty w_l(r, r') \chi_l(k, r') \, dr', \tag{2}$$

wherein $w_l(r, r')$ are the multipoles of the non-local *NA* interaction. We have suppressed all terms due to the intrinsic spin of the system for simplicity of expression. Note, however, that spin–orbit interactions arising from the actual folding process (Amos *et al.* 2000) are taken into account in the calculations.

Solution of the equations (2) (with spin–orbit potentials included) have been evaluated for all of the cases studied using the program DWBA98 (Raynal 1999). With that program, scattering phase shifts and amplitudes can be extracted from which cross sections and analysing powers for *NA* scattering are defined. Note that for non-zero spin targets, non-zero angular momentum transfer amplitudes are included in the calculations, with the associated scattering amplitudes evaluated using a DWA.

To define the non-local interaction for *NA* scattering in the *g*-folding procedure, exchange amplitudes resulting from antisymmetrisation of the complete $A + 1$ nucleon scattering system must be included. Consider the first-order optical potential defined schematically by

$$U_{pA} = \left\langle \Psi(1, 2, \ldots, A) \left| \sum_{n=1}^A g_{eff}(n0) \mathcal{A}(0, n) \right| \Psi(1, 2, \ldots, A) \right\rangle, \tag{3}$$

where '0' denotes the projectile coordinates and $\mathcal{A}(0, n)$ is the antisymmetrisation operator. As all nucleons in the target are equivalent, we can choose a specific entry ('1') and write

$$U_{pA}(01) = A \left\langle \Psi(1, 2, \ldots, A) \left| g_{eff}(10) \mathcal{A}(0, 1) \right| \Psi(1, 2, \ldots, A) \right\rangle; \tag{4}$$

the angle brackets now symbolising the expectation taken over all the states of particles $2, 3, \ldots, A$. A cofactor expansion of the nuclear states,

$$|\Phi_{JM}(1, 2, \ldots, A)\rangle = A^{-\frac{1}{2}} \sum_{\alpha} a_{\alpha} |\Phi_{JM}(1, 2, \ldots, A)\rangle \, |\phi_{\alpha}(1)\rangle, \qquad (5)$$

where $\alpha = \{(nl)\,jm\}$, permits a factorisation of the many-nucleon matrix elements so that for the case $J = 0$, on using the Wigner–Eckart theorem,

$$U_{pA}(01) = \sum_{\alpha\alpha'} \left\langle \Psi_{gs}^{J=0} \middle| a_{\alpha'}^{\dagger} a_{\alpha} \middle| \Psi_{gs}^{J=0} \right\rangle \langle \phi_{\alpha'}(1') | g_{10} | \phi_{\alpha}(1) \rangle$$

$$= \sum_{\alpha\alpha'} [2j + 1]^{-\frac{1}{2}} \left\langle \Psi_{gs}^{J=0} \middle\| \left[a_{\alpha'}^{\dagger} \times \tilde{a}_{\alpha} \right]^{(0)} \middle\| \Psi_{gs}^{J=0} \right\rangle \langle \phi_{\alpha'}(1') | g_{10} | \phi_{\alpha}(1) \rangle. \quad (6)$$

Therein the coordinate $1'$ can be either '1' itself giving the direct term of the optical potential and found when the detected nucleon is the projectile, or '0' leading to the exchange term that results when the detected nucleon originally was bound in the target. The doubly reduced amplitudes,

$$\left\langle \Psi_{gs}^{J=0} \middle\| \left[a_{\alpha'}^{\dagger} \times \tilde{a}_{\alpha} \right]^{(0)} \middle\| \Psi_{gs}^{J=0} \right\rangle,$$

are one-body density matrix elements (OBDME). In general for a ground state expectation those OBDME are defined by

$$S_{\alpha\alpha' I}^{J_{gs}} = \left\langle \Psi_{gs}^{J} \middle\| \left[a_{\alpha'}^{\dagger} \times \tilde{a}_{\alpha} \right]^{(I)} \middle\| \Psi_{gs}^{J} \right\rangle, \qquad (7)$$

and are obtained directly from the shell model wave functions. One can have non-zero angular momentum transfer contributions to elastic scattering. However, for even–even nuclei, as $J_{gs} = I = 0$, the OBDME are expressed simply by

$$\sigma_{\alpha\alpha'} = \frac{1}{2j + 1} S_{\alpha\alpha' 0}^{0}, \qquad (8)$$

where α and α' may differ in the value of n. For $\alpha = \alpha'$, these are fractional shell occupancies of nucleons in the ground state.

Thus the microscopic optical potential takes the form

$$U(\mathbf{r_0}, \mathbf{r_1}; E) = \sum_{\alpha, \alpha'} [2j + 1]^{\frac{1}{2}} \sigma_{\alpha\alpha'} \left[\delta(\mathbf{r_0} - \mathbf{r_1}) \int \phi_{\alpha'}^{*}(\mathbf{s}) U^{(D)}(r_{0s}) \phi_{\alpha}(\mathbf{s}) \, d\mathbf{s} \right.$$

$$\left. + \phi_{\alpha'}(\mathbf{r_0}) U^{(Ex)}(r_{01}) \phi_{\alpha}(\mathbf{r_1}) \right], \qquad (9)$$

where $r_{01} = |\mathbf{r_0} - \mathbf{r_1}|$ and $U^{(D)}$ and $U^{(Ex)}$ are combinations of the multipoles of the effective *NN* interactions as one deals with the direct and exchange elements of the folding process.

(2b) Effective NN Interactions

The effective *NN* interactions for 25, 30 and 40 MeV incident protons are a mix of central, two-body spin–orbit, and tensor attributes each having a form factor that is a sum

of Yukawa functions (Dortmans and Amos 1994) with complex, energy- and density-dependent strengths obtained by accurately mapping their double Bessel transforms to the (*NN*) *g*-matrices of the Bonn-B potential (Machleidt *et al.* 1987). Those *g*-matrices are the solutions of the Bethe-Brueckner–Goldstone equations for energy $E \to k^2$ and for diverse Fermi momenta, k_F,

$$g_{LL'}^{JST}(p', p; k, K, k_F)$$

$$= V_{LL'}^{JST}(p, p') + \frac{2}{\pi} \sum_l \int_0^\alpha V_{Ll}^{JST}(p', q) \left\{ \frac{\bar{Q}(q, K, k_f)}{\bar{E}(k, K, k_f) - \bar{E}(q, K, k_f) + i\epsilon} \right\}$$

$$\times g_{lL'}^{(JST)}(q, p; k, K, k_F) q^2 \, dq, \tag{10}$$

in which $\bar{Q}(q, K, k_f)$ is an angle-averaged Pauli operator and $\bar{E}$ are single particle energies, all evaluated at an average centre-of-mass momentum K (Dortmans and Amos 1991). The energy and density dependence of the complex effective *NN* interactions so formed have been crucial in forming the optical potentials that yield good predictions at 65 and 200 MeV (Dortmans *et al.* 1997, 1998).

3. Results of Calculations

We display the results of our calculations of the elastic scattering of 25, 30 and 40 MeV protons from many target nuclei in the following five subsections; the first three dealing with data for each particular energy separately. In the fourth we discuss energy, and in the fifth isotope variations. In most of the cases we have used harmonic oscillator (HO) functions for the bound state single particle functions, but for light nuclei, ^{6}Li in particular, we have used Wood–Saxon (WS) potential functions. The oscillator length for the HO functions was set by an $A^{1/6}$ rule as indicated as reasonable by electron scattering studies.

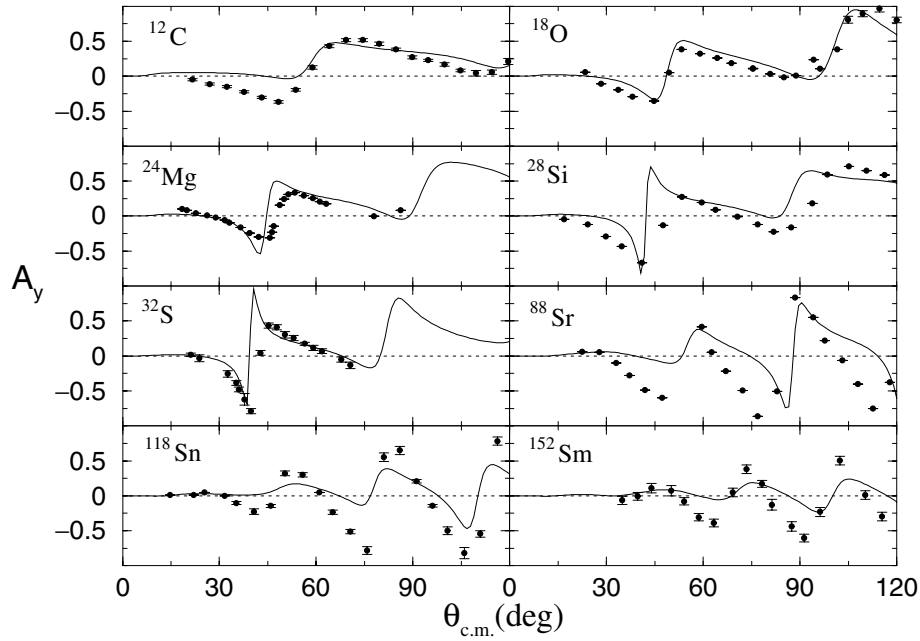### (3a) Results of the Scattering of 25 MeV Protons

The results of our calculations of the elastic scattering of 25 MeV (and adjacent energies) protons from different nuclei are shown in Figs 1–3. In Fig. 1, calculations of proton scattering from the nuclei ^{6,7}Li, ^{12}C, ^{14}N, ^{18}O, ^{24}Mg, ^{27}Al and ^{28}Si are compared with the experimental data. Data were measured at 25.9 MeV for ^{6}Li (Mughrabi *et al.* 1984), at 24.4 MeV for ^{7}Li (Petrovich *et al.* 1993), at 24 MeV for ^{12}C (Knöpfle *et al.* 1973), at 26 MeV for ^{14}N (Lutz *et al.* 1972), at 24.5 MeV for ^{18}O (Escudié *et al.* 1974), at 27 MeV for ^{24}Mg (Roy *et al.* 1983), at 28 MeV for ^{27}Al (Dittman *et al.* 1969), and at 25 MeV for ^{28}Si (Lamontagne *et al.* 1973). In the ^{6}Li case, the calculated results are in very good agreement with the experimental data up to 120° scattering. For the other cases, however, while the shapes of the calculated results are quite similar to those of experimental data, the minima are over-accentuated, and this over-accentuation increases with the target mass. In Fig. 2, our predictions for 25 MeV proton scattering from the nuclei ^{40,48}Ca, ^{58}Cu, ^{88}Sr, ^{89}Y, ^{152}Sm, ^{232}Th and ^{238}U are compared with the experimental data. Data were measured at 25 MeV for ^{40,48}Ca (McCamis *et al.* 1986), at 28 MeV for ^{58}Cu (Dittman *et al.* 1969), at 24.6 MeV for ^{88}Sr (Wassenaar *et al.* 1989), at 25 MeV for ^{89}Y (Austin 1967) and for ^{152}Sm (Barbier *et al.* 1971), and at 26 MeV for ^{232}Th and for ^{238}U (Hansen *et al.* 1982). The ^{40,48}Ca and ^{58}Cu results agree reasonably with observation, although our predictions again give too sharp a structure and have the maxima and minima at slightly too large scattering angles. For ^{88}Sr and more particularly ^{89}Y, the data are well reproduced to quite
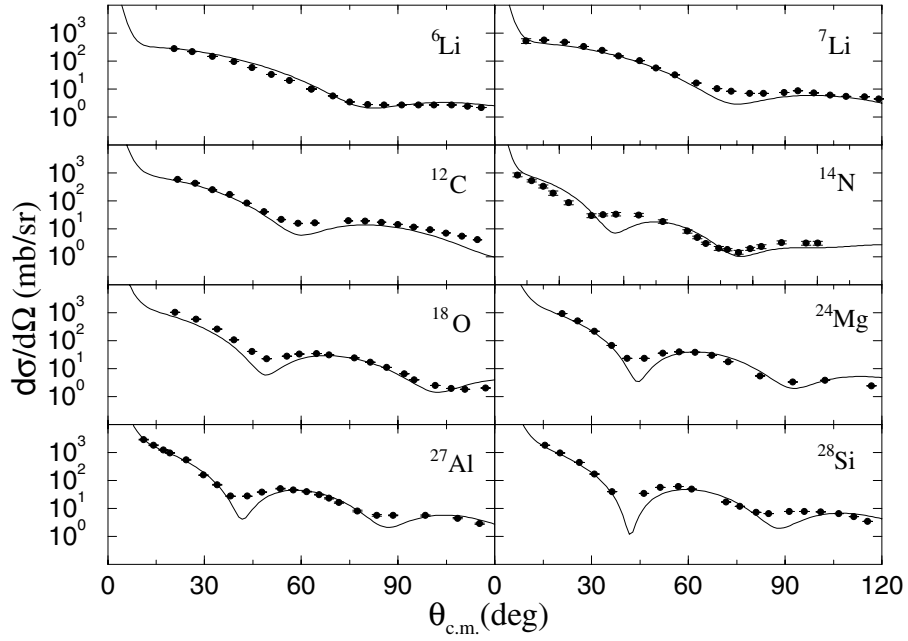
Fig. 1. The differential cross sections from the elastic scattering of 25 MeV protons from ^{6,7}Li, ^{12}C,^{14}N, ^{18}O, ^{24}Mg, ^{27}Al and ^{28}Si. Data (dots) are compared with the results of our microscopic model calculations (solid curves).
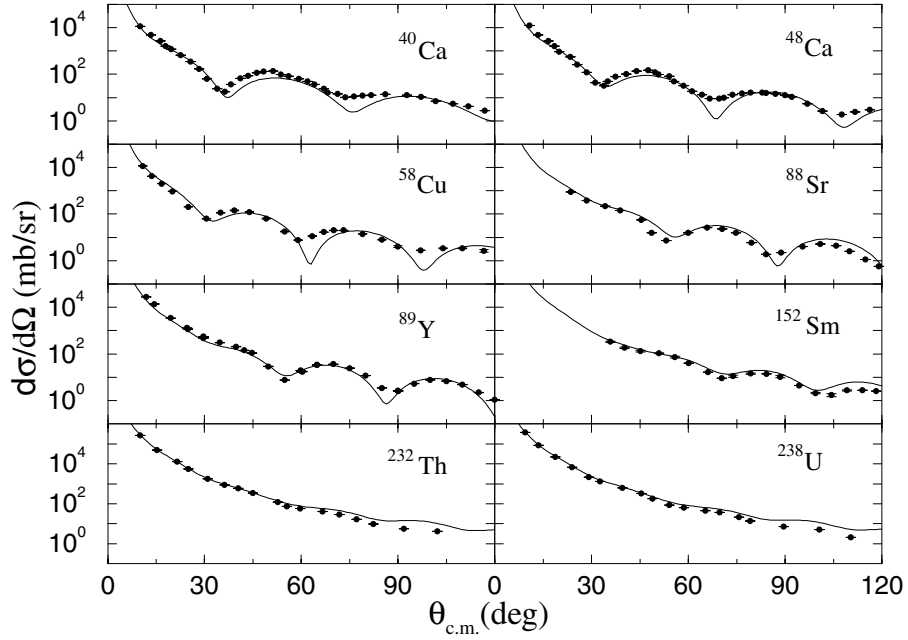
Fig. 2. As for Fig. 1, but for ^{40,48}Ca, ^{58}Cu, ^{88}Sr, ^{89}Y, ^{152}Sm, ^{232}Th and ^{238}U.

Fig. 3. The analysing powers from the elastic scattering of 25 MeV protons from ^{12}C, ^{18}O, ^{24}Mg, ^{28}Si, ^{32}S, ^{88}Sr, ^{118}Sn and ^{152}Sm. Data (dots) are compared with the predictions found from microscopic optical potentials.

large scattering angles. That is the case also with ^{152}Sm up to 90°. For the heavy nuclei ^{232}Th and ^{238}U, our predictions are in good agreement with the experimental data up to 60°. For most cases at the larger scattering angles, our results depart from observation, though the shapes of our cross-section predictions remain quite similar to the data.

The 25 MeV elastic proton scattering analysing power data are compared with the results obtained from our optical model calculations in Fig. 3. Analysing power data are compared with our calculated results for the target nuclei as indicated in each segment. Data were measured at 24.1 MeV for ^{12}C (Craig *et al.* 1966), at 24 MeV for ^{18}O (Escudié *et al.* 1974), at 25 MeV for ^{24}Mg (Roy *et al.* 1983), ^{28}Si (Lamontagne *et al.* 1973) and ^{32}S (Roy *et al.* 1983), at 24.6 MeV for ^{88}Sr (Wassenaar *et al.* 1989), and at 24.5 MeV for ^{118}Sn (Tarrats *et al.* 1981) and ^{152}Sm (Barbier *et al.* 1971). For the light mass nuclei ($A \leq 40$), the shape and size of the data are very similar to our predictions. For heavier nuclei, our predictions tend to under-estimate the magnitude variation in the data, particularly so for ^{152}Sm. Results of the predictions of the other isotopes of calcium are presented later.
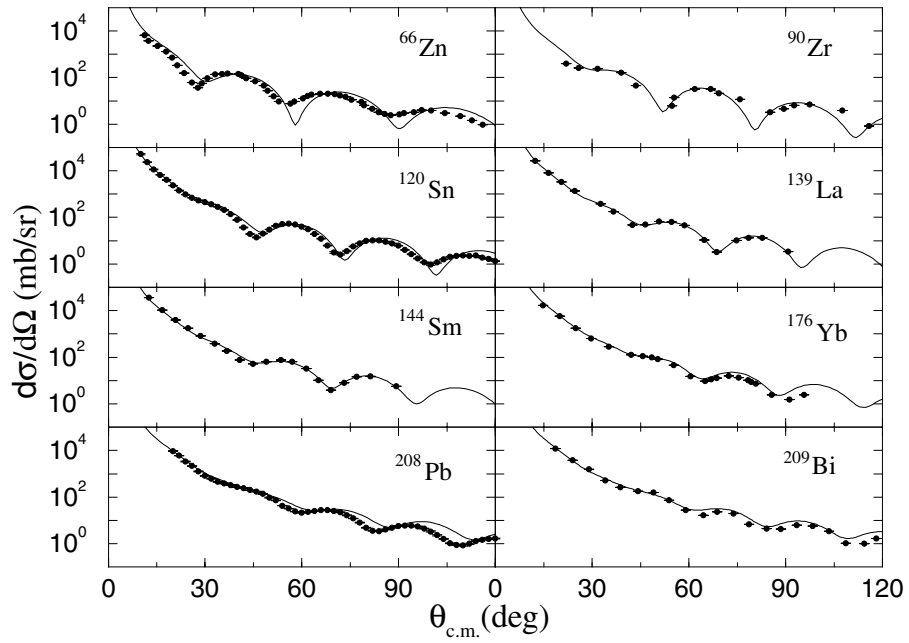
(3b) Results of the Scattering of 30 MeV Protons

We present our results of the optical model calculations of 30 MeV proton scattering from different nuclei in Figs 4–7. In Fig. 4 the differential cross sections from ^{10}B, ^{13}C, ^{16}O, ^{20}Ne, ^{40}Ar, ^{56}Fe, ^{58}Ni and ^{63}Cu are compared with the experimental data. Differential cross-section data were measured (Votava *et al.* 1973; Pham and de Swiniarski 1977) at 30.3 MeV for ^{10}B, ^{16}O and ^{20}Ne. For ^{13}C data were taken at 30.5 MeV (Greaves *et al.* 1972) and at 30 MeV for ^{40}Ar (Rush *et al.* 1971) and at 30.3 MeV for ^{56}Fe and ^{58}Ni (Ridley and
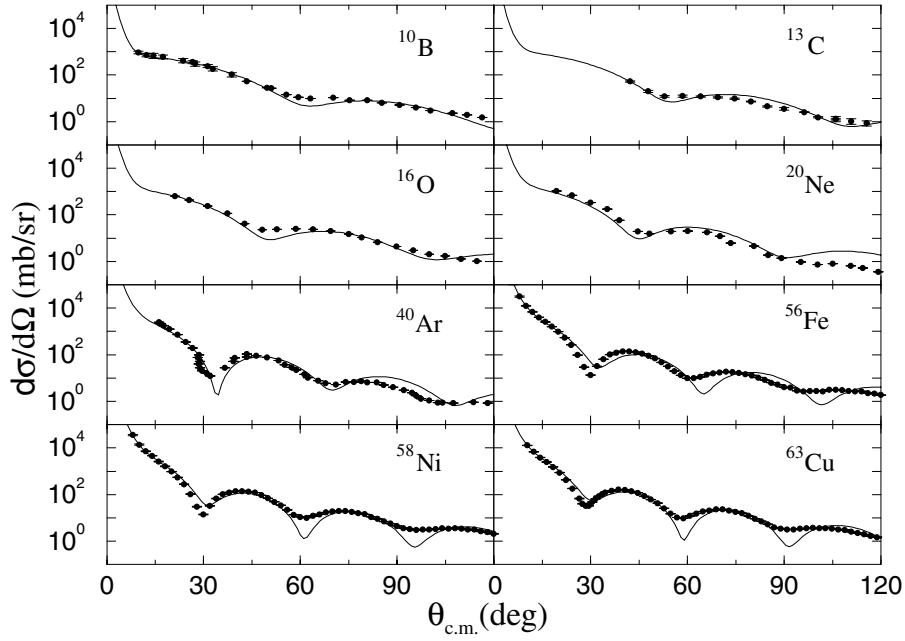
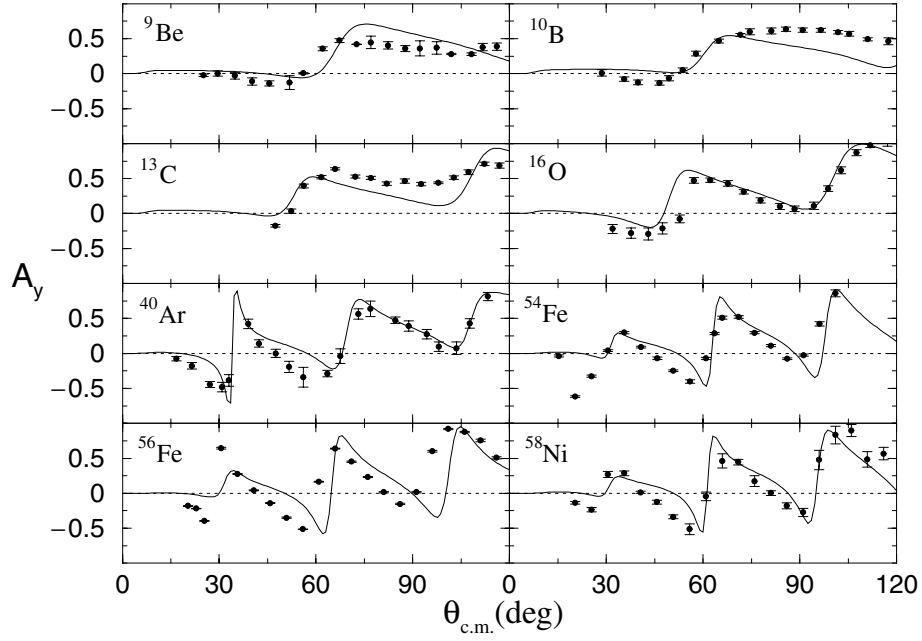**Fig. 4.** The differential cross sections from the elastic scattering of 30 MeV protons from ^{10}B, ^{13}C, ^{16}O, ^{20}Ne, ^{40}Ar, ^{56}Fe, ^{58}Ni and ^{59}Co. The data (dots) are compared with the predictions (solid curves) obtained using *g*-folding optical potentials.

Fig. 5. As for Fig. 4, but for ^{66}Zn, ^{90}Zr, ^{120}Sn, ^{139}La, ^{144}Sm, ^{176}Yb, ^{208}Pb and ^{209}Bi.

Fig. 6. The analysing powers from the elastic scattering of 30 MeV protons from ^{9}Be, ^{10}B, ^{13}C, ^{16}O, ^{40}Ar, ^{54}Fe, ^{56}Fe and ^{58}Ni. The data (dots) are compared with the optical potential results (solid curves).
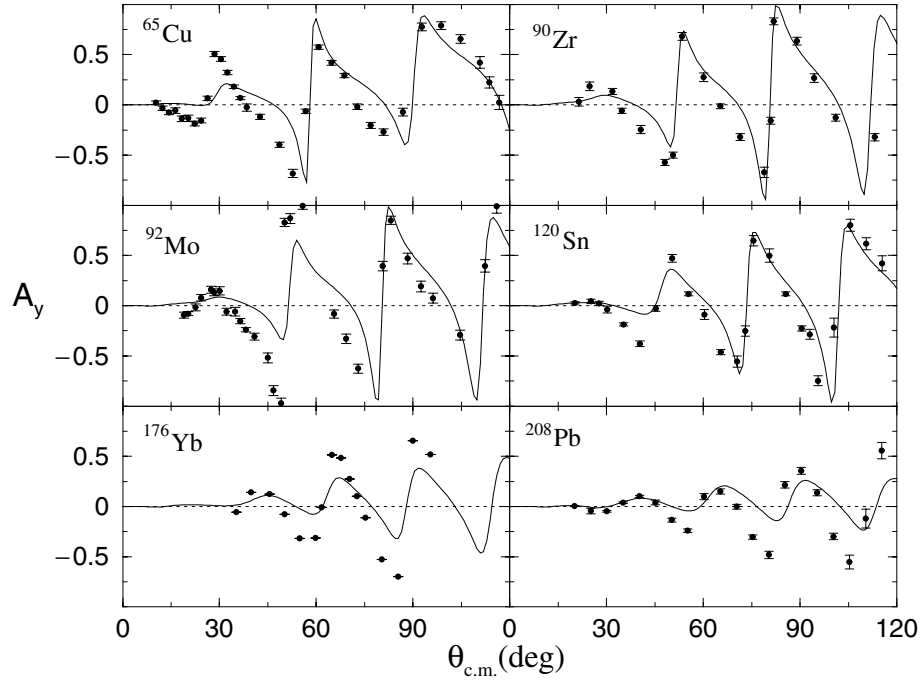
Fig. 7. As for Fig. 6, but for ^{65}Cu, ^{90}Zr, ^{92}Mo, ^{120}Sn, ^{176}Yb and ^{208}Pb.

Turner 1964). The shapes of the experimental data are well reproduced by our calculations, but the minima in the data from the heavier targets are too sharply predicted. These effects concur with our results from the 25 MeV analyses.

In Fig. 5 the results of our calculations of scattering from ^{66}Zn, ^{90}Zr, ^{120}Sn, ^{139}La, ^{144}Sm, ^{176}Yb, ^{208}Pb and ^{209}Bi are compared with the respective differential cross-section data. Data were measured at 30 MeV for ^{90}Zr (de Swiniarski *et al.* 1977), at 30.5 MeV for ^{66}Zn (Tait *et al.* 1971), at 30.3 MeV for ^{120}Sn and ^{208}Pb (Ridley and Turner 1964), at 29.32 MeV for ^{139}La (Helten *et al.* 1973), at 30 MeV for ^{144}Sm (Helten *et al.* 1973) and ^{176}Yb (Kamigaito *et al.* 1988), and at 31 MeV for ^{209}Bi (Sandhu 1970). The results of scattering from ^{66}Zn are quite similar to those obtained from ^{65}Cu and ^{68}Zn (not shown), and the first-order minima in the data are under-estimated by the calculations but the higher-order minima are over-estimated. Nevertheless, the shapes of those cross sections are still well reproduced. With scattering from ^{90}Zr, data are well replicated in the measured range (30° to 100°). For all of the tin isotopes (only ^{120}Sn is shown in Fig. 5), data are well reproduced up to 40° scattering. At larger scattering angles, the shape of the calculated results are similar to the data but the successive minima are more sharply defined than indicated by the data. Our calculated results are in excellent agreement with the experimental data from ^{139}La, ^{144}Sm, ^{176}Yb and ^{209}Bi. For ^{208}Pb, our predictions over-estimate the cross-section data at large scattering angles which seems to us a reflection of an inadequacy in the chosen model of structure. Consideration of an alternative structure specification for the ground state of ^{208}Pb is under study at present. The cross sections from ^{9}Be, ^{11}B, ^{19}F, ^{21}Ne, ^{54}Fe, ^{59,60}Co, ^{65}Cu, ^{68}Zn, ^{104}Ru, ^{112,114,116,118,122,124}Sn and ^{141}Pr have also been found and, when compared with data, are as good if not better than those shown in Figs 4 and 5. Some of these are displayed later.

In Figs 6 and 7 we present the results of our calculations for the analysing powers from the elastic scattering of 30 MeV protons from all the nuclei whose cross sections were given in the preceding figures. Our calculated analysing powers show the trend of the data for the lightest mass targets (the ^{9}Be results are given here to stress that problems are not so severe), but quite good agreement is found for targets ranging from ^{16}O to ^{58}Ni. That agreement remains with the data from ^{65}Cu to ^{120}Sn, although for these targets predictions tend to under-estimate the data in the angle range 20° to 60° and also the characteristic forward (negative value) peak. While the data from heavier nuclear targets are not as sharply structured as that from lighter nuclei, our calculations gave more compressed values. We find that the general structure of the ^{176}Yb and ^{208}Pb analysing powers are matched in calculation, but the peak magnitudes are at best half of the measured ones.

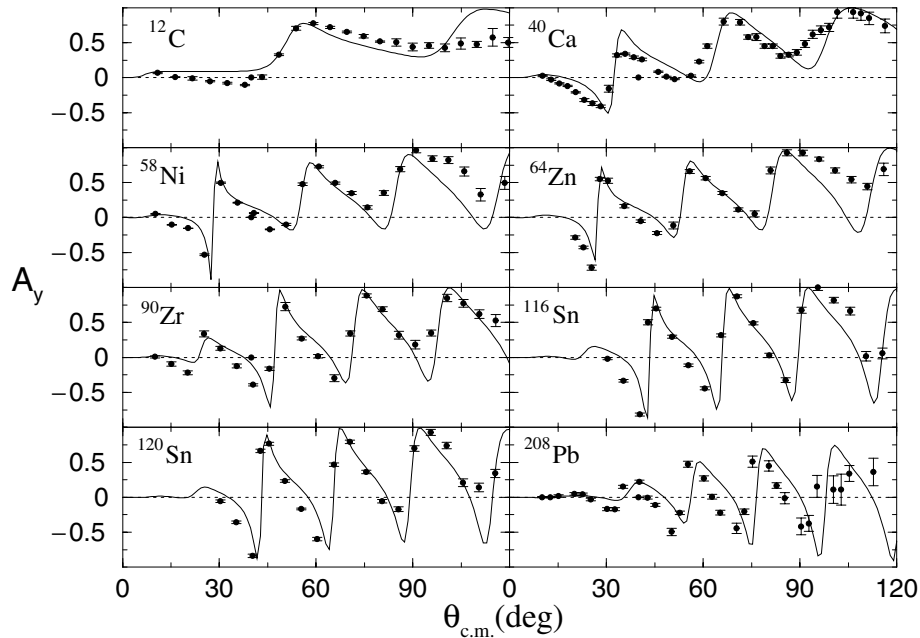*(3c) Results of the Scattering of 40 MeV Protons*

The results obtained from our optical model calculations of the elastic scattering of 40 MeV protons from targets of different nuclei are compared with data in Figs 8–10. In Fig. 8 the cross sections from ^{6}Li, ^{12}C, ^{16}O, ^{24}Mg, ^{27}Al and ^{28}Si are compared with the experimental data. Data were measured at 40 MeV for ^{6}Li (Bray *et al.* 1972), ^{12}C (Blumberg *et al.* 1966), ^{24}Mg (Zuffi *et al.* 1986), ^{27}Al and ^{28}Si (Sandhu 1970), and at 39.7 MeV for ^{16}O (Delaroche *et al.* 1986). Calculations are in good agreement with the data; much better in fact than for the 25 and 30 MeV studies. At the larger scattering angles, however, the predictions still have slightly more defined minima than are evident with the data. The results found for 40 MeV proton scattering from ^{40}Ca, ^{58}Ni, ^{64}Zn, ^{90}Zr, ^{120}Sn and ^{208}Pb are compared with the data in Fig. 9. Data were measured at 40 MeV for ^{40}Ca, ^{58}Ni, ^{90}Zr and ^{208}Pb (Blumberg *et al.* 1966) and at 39.6 MeV for ^{64}Zn (Liers *et al.* 1970) and ^{120}Sn (Boyd and
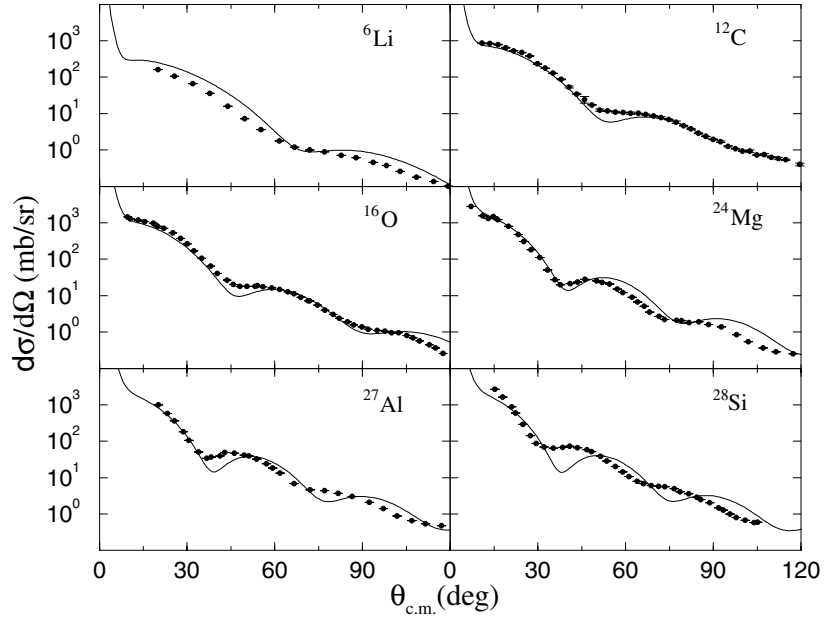
Fig. 8. The differential cross sections from the elastic scattering of 40 MeV protons from ^{6}Li, ^{12}C, ^{16}O, ^{24}Mg, ^{27}Al and ^{28}Si. Data (dots) are compared with the calculated results found using *g*-folding optical potentials (solid curves).
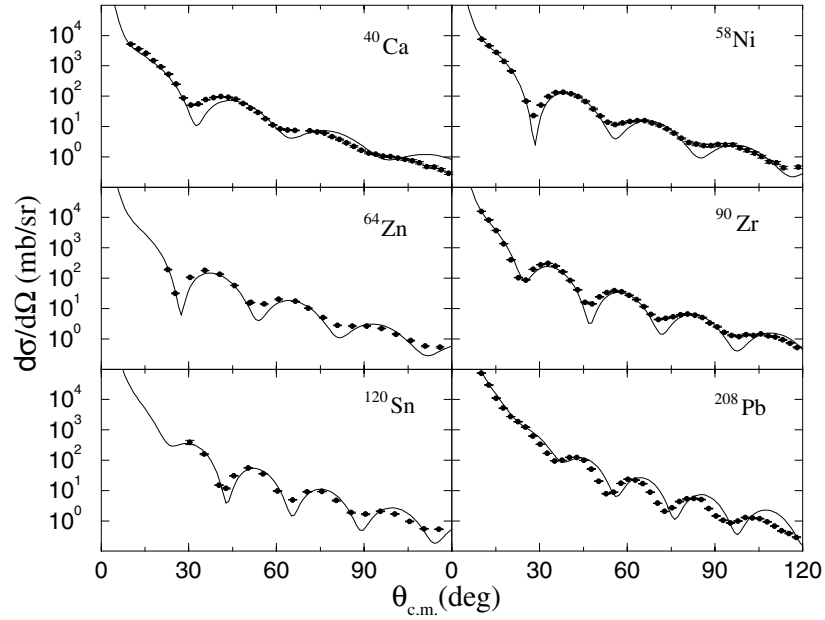
Fig. 9. As for Fig. 8, but for ^{40}Ca, ^{58}Ni, ^{64}Zn, ^{90}Zr, ^{120}Sn and ^{208}Pb.

Fig. 10. The analysing powers from the elastic scattering of 40 MeV protons from ^{12}C, ^{40}Ca, ^{58}Ni, ^{64}Zn, ^{90}Zr, ^{116,120}Sn and ^{208}Pb. Data are displayed by the dots, while the results of our optical potential calculations are shown by the solid curves.

Greenlees 1968). Although most have sharply defined minima, the calculations agree with data quite well. They are in good agreement with the shape and magnitudes of the cross-section data and up to 120° scattering in most cases. This quality of the predicted results was found previously for higher energy studies, and at 65 MeV in particular (Dortmans *et al.* 1998). That remains the case with the results we have found for 40 MeV proton scattering from other nuclei, namely ^{15}N, ^{27}Al, ^{92}Zr and the other isotopes of nickel, zinc and tin. Some of those other results will be given in the following subsections.

In Fig. 10 the analysing powers associated with 40 MeV proton scattering from ^{12}C, ^{40}Ca, ^{58}Ni, ^{64}Zn, ^{90}Zr, ^{116,120}Sn and ^{208}Pb are compared with the experimental data (Liers *et al.* 1970; Blumberg *et al.* 1966; de Swiniarski *et al.* 1977, 1979; Boyd and Greenlees 1968). The predictions and data from all targets at 40 MeV are in agreement almost as good as that found with the 65 and 200 MeV studies. However, the ^{208}Pb results are slightly at odds with observation; a feature we consider again to be due to the inadequacy of the assumed target structure. However, the degree of compression of the ^{208}Pb data (from analysing power peak sizes of ± 1) now compares quite well that predicted. It is the mismatch of the angle values at which the zeros occur that we note as possible evidence for the inadequacy of the simple packed orbit model of structure that has been used.

(3d) Energy Variation of the Scattering Data

The energy variation of the cross-section and analysing power data, and of the results obtained using our *g*-folding optical potentials, for proton elastic scattering from ^{40}Ca at 25 and 40 MeV and from ^{58}Ni at 30.3 and 40 MeV are shown in Fig. 11. The data for ^{90}Zr, ^{120}Sn and ^{208}Pb for 30 and 40 MeV protons are given in Fig. 12.
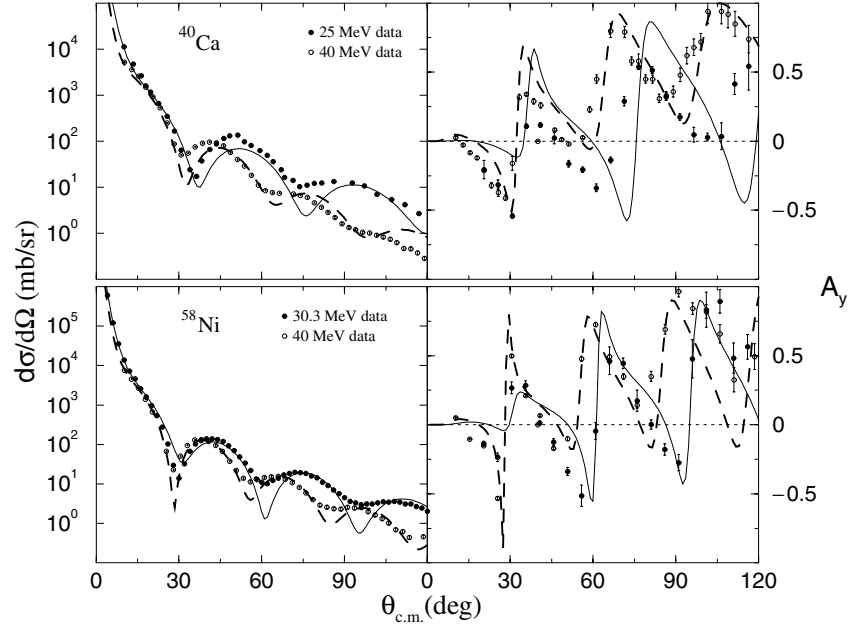
Fig. 11. Energy variation of the differential cross sections and analysing powers for proton scattering for 25 and 40 MeV from ^{40}Ca (top) and for 30.3 and 40 MeV from ^{58}Ni (bottom).
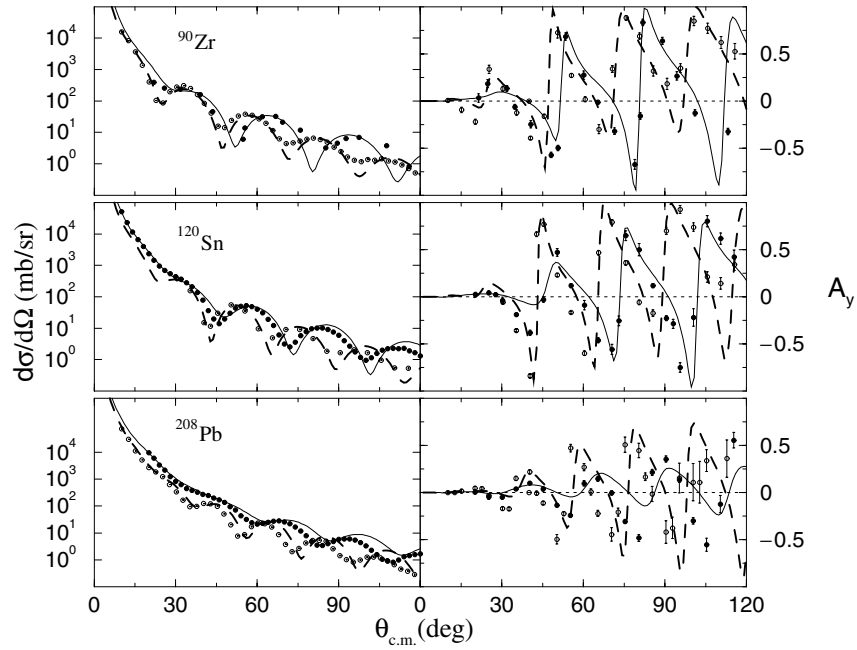
Fig. 12. As for Fig. 11, but for the scattering of 30 and 40 MeV protons from ^{90}Zr (top), ^{120}Sn (middle) and ^{208}Pb (bottom).

In Fig. 11 the 25 and 40 MeV results are shown for ^{40}Ca by the solid dots and curves, while the 40 MeV data are presented by the open dots with our calculated results displayed by the dashed curves. With the ^{58}Ni results, the notation differs only in that the energies are 30.3 and 40 MeV. It is evident that the general pattern of change in both the cross-section and analysing power data from these nuclei is reproduced with the calculations; the more so with ^{58}Ni. In the ^{40}Ca case, the 25 MeV results are most at odds with observation. Of particular note in the cross sections is that the positions, and in case of ^{58}Ni particularly the peak sizes, are correctly found. That is also the case with the analysing powers, with our calculations for ^{58}Ni following the positions and size variations of the maxima in the data quite well. Such variations are equally evident with the results given in Fig. 12. Now the sizes and positions of the peaks in the cross sections from ^{90}Zr and ^{120}Sn are quite well predicted, while those in the cross-section data from ^{208}Pb are slightly shifted at both energies. The analysing power data trends are well followed also, particularly the relative size changes of the data with energy to 60° in the case of ^{120}Sn. As with the cross-section comparisons, for the calculated ^{208}Pb analysing power there is a mismatch with observation; the calculated maxima at both energies occur at slightly larger scattering angles than that seen in the data. But the general variation of sizes of the analysing power data at the two energies is evident with the calculations.

The problem with the 25 MeV ^{40}Ca results could be attributed to effects such as virtual excitation of giant resonances, given that the giant dipole excitation is near 25 MeV in mass 40 nuclei (Berman 1975). At 30 MeV for the other nuclei, and at 40 MeV for all five nuclei considered, such competing processes in elastic scattering are not favoured. Since the discrepancies between the data and results found for ^{208}Pb appear constant with energy, it seems that our choice of (simple shell) model for the structure of the nucleus has been poor.

*(3e) The Isotope Variation of the Scattering Data*

We present the variations with isotope of the target nucleus of data and calculated results in Figs 13–15. In Fig. 13 the cross sections for 25 MeV proton scattering from ^{40,42,44,48}Ca are shown in the top segments, while those from 30.3 MeV protons scattering from ^{112,116,120,122,124}Sn (Hardacre *et al.* 1971) are given in the bottom panels. In both cases the data are shown in the left-hand sectors with lines drawn through to guide the eye, while the calculated cross sections are presented on the right. With ^{40}Ca, we know from the above that the calculated result is not in as good agreement with the data as we have found in almost all other cases. But these results demonstrate that the trend with mass is viable. We expect that any competing process, e.g. virtual excitation of giant resonance, would be similar for all of these calcium isotopes at 25 MeV. With the tin isotopes, the trend with increasing neutron number seen in the data is reflected in our calculated results with only the ^{112}Sn result being slightly out in angular form.

In Fig. 14 the 40 MeV cross sections and analysing powers for the nickel isotopes ^{58,60,62,64}Ni are shown. Again the data with lines to guide the eye are given in the left panels, while the results of our calculations are shown on the right. Although our calculated results have more sharply defined structure than the data, they do show the mass variation trend of the data and now with very reasonable peak values in both cross sections and analysing powers. That is also the case with 39.6 MeV proton scattering from the tin isotopes ^{116,118,120,122,124}Sn, as is evident in Fig. 15. Again the data are given in the left panels and the calculated results on the right.
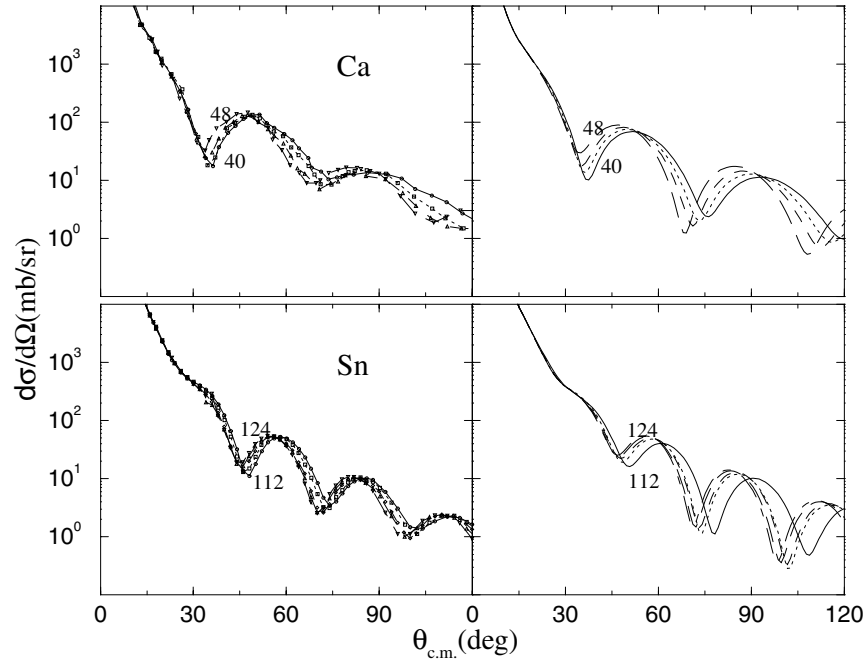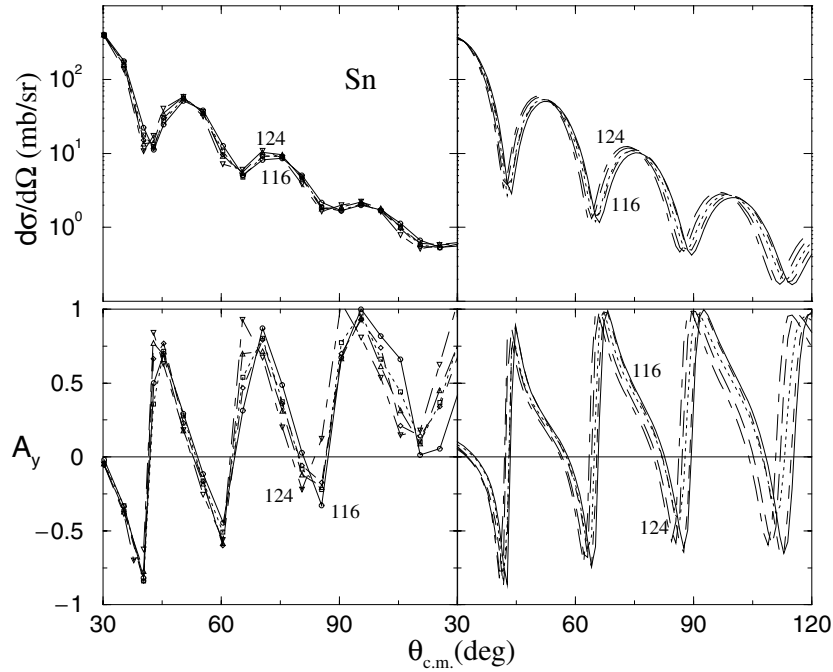
Fig. 13. Differential cross sections from the elastic scattering of 25 MeV protons from ^{40,42,44,48}Ca (top), and of 30.3 MeV protons from ^{112,116,120,122,124}Sn (bottom).
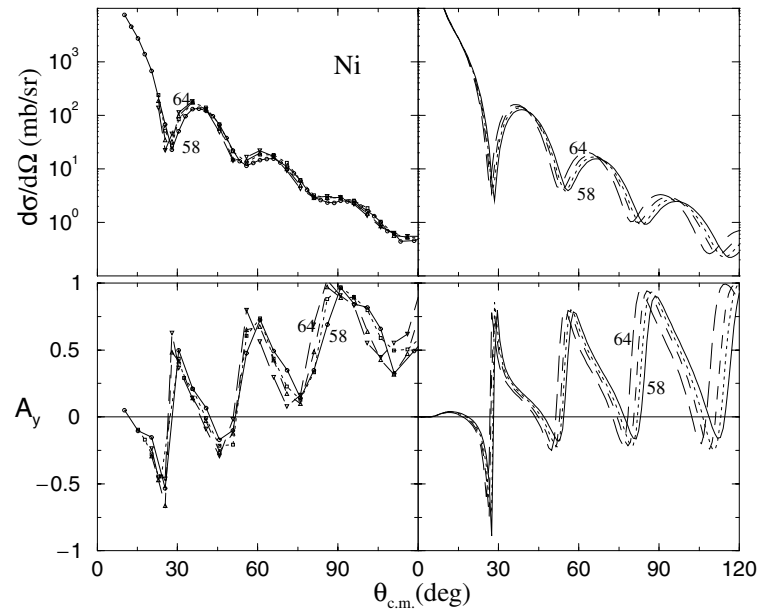
Fig. 14. Differential cross sections (top) and analysing powers (bottom) from the elastic scattering of 40 MeV protons from ^{58,60,62,64}Ni.

Fig. 15.   As for Fig. 14, but for the elastic scattering of 39.6 MeV protons from ^{116,118,120,122,124}Sn.

4. Conclusions

The cross-section and analysing power results obtained from the coordinate space non-local optical potentials formed by *g*-folding at 25, 30 and 40 MeV are in quite reasonable agreement with the data obtained with targets of mass 6 to 238. In general the cross-section predictions give the magnitudes and trends of the peaks in the data but the minima are too sharply defined. While comparisons between the calculated results and the data remain reasonable, for 25 and 30 MeV proton elastic scattering in particular, the disparities are more pronounced than at higher energies (Amos *et al.* 2000). Nevertheless, the *g*-folding optical potentials remain a reasonable first approximation, sufficiently so that the results may still select between different structure inputs. Also the associated distorted wave functions and effective interactions should still be appropriate for use in DWA analyses of inelastic scattering from stable nuclei (Karataglidis *et al.* 1997), or of radioactive beam ions (Lagoyannis *et al.* 2001), as well as of other reaction calculations (Richter *et al.* 1996).

Acknowledgment

References

Amos, K., Dortmans, P. J., Karataglidis, S., Raynal, J., and von Geramb, H. V. (2000). *Adv. Nucl. Phys.* **25**, 275.

Auger, F., *et al.* (1999). Conf. on Experimental Nuclear Physics in Europe, ENPE '99, Seville, Spain.

Austin, S. (1967). Private communication.

Barbier, M. P., Lombard, R. M., Moss, J. M., and Terrien, Y. D. (1971). *Phys. Lett.* B **34**, 386.

Bray, K. H., *et al.* (1972). *Nucl. Phys.* A **189**, 35.

Berman, B. L. (1975). At. Data Nucl. Data Tables **15**, 319.

Blumberg, L. N., Gross, E. E., Van Der Woude, A., Zucker A., and Bassel, R. H. (1966). *Phys. Rev.* **147**, 812.

Boyd, R. N., and Greenlees, G. W. (1968). *Phys. Rev.* **176**, 1394.

Craig R. M., *et al.* (1966). *Nucl. Phys.* **79**, 177.

Deb, P. K., and Amos, K. (2000). *Phys. Rev.* C **62**, 024605.

Deb, P. K., Amos, K., and Karataglidis, S. (2000). *Phys. Rev.* C **62**, 037601.

Delaroche, J. P., Islam, M. S., and Finlay, R. W. (1986). *Phys. Rev.* C **33**, 1826.

de Swiniarski, R., Pham, D. L., and Bagieu, G. (1977). *Can. J. Phys.* **55**, 43.

de Swiniarski, R., Pham, D. L., Bagieu, G., and von Geramb, H. V. (1979). *Can. J. Phys.* **57**, 540.

Dittman, R., Sandhu, H. S., Cole R. K., and Waddell, C. M. (1969). *Nucl. Phys.* A **126**, 592.

Dortmans, P. J., and Amos, K. (1991). *J. Phys.* G **17**, 901.

Dortmans, P. J., and Amos, K. (1994). *Phys. Rev.* C **49**, 1309.

Dortmans, P. J., Amos, K., Karataglidis, S., and de Swiniarski, R. (1995). *Phys. Rev.* C **52**, 3224.

Dortmans, P. J., Amos, K., and Karataglidis, S. (1997). *J. Phys.* G **23**, 183.

Dortmans, P. J., Amos, K., Karataglidis, S., and Raynal, J. (1998). *Phys. Rev.* C **58**, 2249.

Escudié, J. L., Lombard, R., Pignanelli, M., Resmini, F., and Tarrats, A. (1974). *Phys. Rev.* C **10**, 1645.

Greaves, P. D., Hnizdo, V., Lowe, J., and Karban, O. (1972). *Nucl. Phys.* A **179**, 1.

Hansen, L. F., Proctor, I. D., Heikkinen, D. W., and Madsen, V. A. (1982). *Phys. Rev.* C **25**, 189.

Hardacre, A. G., Turner, J. F., Kerr, J. C., Grad, G. A., Cavanagh, P. E., and Coleman, C. F. (1971). *Nucl. Phys.* A **173**, 436.

Helten, V. D., Hilbert, J. C., and Ball, J. B. (1973). *Nucl. Phys.* A **201**, 225.

Kamigaito, O., *et. al.* (1988). RCNP Annual Report, p. 16.

Karataglidis, S., Brown, B. A., Dortmans, P. J., and Amos, K. (1997). *Phys. Rev.* C **55**, 2826.

Knöpfle, K. T., Ingham, D., Rogge, M., and Mayer-Böricke, C. (1973). Annual Report. KFA-IKP 10/74 KFA, Jülich, Germany.

Lamontagne, C. R., *et al.* (1973). *Phys. Lett.* **B45**, 465.

Lagoyannis, A., *et al.* (2001). nucl-ex/0004001 and *Phys. Lett.* (submitted).

Liers, H. S., Boyd, R. N., Poppe, C. H., Sievers, J. A., and Watson, D. L. (1970). *Phys. Rev.* C **2**, 1399.

Lutz, H. F., Heikkinen, D. W., and Bartolini, W. (1972). *Nucl. Phys.* A **198**, 257.

McCamis, R. H., *et al.* (1986). *Phys. Rev.* C **33**, 1624.

Machleidt, R., Hollinde, K., and Elster, Ch. (1987). *Phys. Rep.* **149**, 1.

Mueller, A. C. (1999). *Nucl. Phys.* A **654**, 215c.

Mughrabi, B. A., El Itaoui, Z., Ellis, P. J., and Tang, Y. C. (1984). *Phys. Rev.* C **29**, 29.

Petrovich, F., *et al.* (1993). *Nucl. Phys.* A **563**, 387.

Pham, D. L., and de Swiniarski, R. (1977). *Nuovo Cimento* A **41**, 543.

Raynal, J. (1999). Computer Code DHBA98, NEA 1209/05.

Richter, W. A., *et al.* (1996). *Phys. Rev.* C **54**, 1756.

Ridley, B. W., and Turner, J. F. (1964). *Nucl. Phys.* A **58**, 497.

Roy, R., *et al.* (1983). *Nucl. Phys.* A **411**, 1.

Rush, A. A., Burge, E. J., and Smith, D. A. (1971). *Nucl. Phys.* A **166**, 378.

Sandhu, H. S. (1970). *Nucl. Phys.* A **146**, 163.

Sandhu, H. S., Cameron, J. M., and Mcgill, W. F. (1971). *Nucl. Phys.* A **169**, 600.

Tait, W. H., Burge E. J., and Edwards, V. R. W. (1971). *Nucl. Phys.* A **176**, 390.

Tanihata, T. (1999). *Nucl. Phys.* A **654**, 235c.

Tarrats, A., Escudié, J. L., and Brissaud, I. (1981). *Nucl. Phys.* A **362**, 128.
von Geramb, H. V., *et al*. (1975). *Phys. Rev.* C **12**, 1697.
Votava, H. J., Clegg, T. B., Ludwig, E. J., and Thompson, W. J. (1973). *Nucl. Phys.* A **204**, 529.
Wassenaar, S. D., *et al*. (1989). *J. Phys.* G **15**, 181.
Zuffi, L., Maino, G., and Ventura, A. (1986). *Phys. Rev.* C **34**, 1223.